Dynamics of a magnetic dimer with exchange, dipolar and Dzyalozhinski-Moriya interaction

A. F. Franco, J.M. Martinez, J.L. Déjardin, and H. Kachkachi
LAMPS, Université de Perpignan Via Domitia, 52 avenue Paul Alduy, F-66860 Perpignan Cedex, France

We investigate the dynamics of a magnetic system consisting of two magnetic moments coupled by either exchange, dipole-dipole, or Dzyalozhinski-Moriya interaction. We compare the switching mechanisms and switching rates as induced by the three couplings. For each coupling and each configuration of the two anisotropy axes, we describe the switching modes and, using the kinetic theory of Langer, we provide (semi-)analytical expressions for the switching rate. We then compare the three interactions with regard to their efficiency in the reversal of the net magnetic moment of the dimer. We also investigate how the energy barriers vary with the coupling. For the dipole-dipole interaction we find that the energy barrier may either increase or decrease with the coupling depending on whether the latter is weak or strong. Finally, upon comparing the various switching rates, we find that the dipole-dipole coupling leads to the slowest magnetic dimer, as far as the switching of its net magnetic moment is concerned.

I. INTRODUCTION

Multilayered magnetic systems as permanent magnets with high performances encounter a renewed interest due to their potential use as magnetic recording media with high thermal stability and reduced switching fields[1–3]. Another candidate for information storing media, also of constantly growing interest, is provided by magnetic nanoparticles. For such applications, it is very important to understand how the dynamics of these systems and their reversal mechanisms are altered by a change in their physical parameters such as the underlying material, thickness, and stacking conditions. There are also rather involved issues related with surface and interface effects even if one assumes, to some extent, that the problems of crystalline diffusion are properly dealt with during fabrication. Apart from the issues related with the intrinsic properties of the constituting elements (layers or particles), an issue of paramount importance is that of (inter-layer or inter-particle) interactions as these affect energy barriers which they have to circumvent during their switching process. Now, because the latter play a central role in magnetic recording technology, the problem of interactions must be addressed in a broader way. Indeed, several types of interactions may occur in particle ensembles or in multi-layered systems. However, it is a difficult task, if at all possible, to tell in detail what interactions are involved in the dynamics of the systems to be studied. In general, one resorts to the "molecular field" approach and considers only the effective interaction. On the other hand, it is clear that the dynamics strongly depends on the type of interaction that is operating within the system. As such, it would be useful to relate the observed dynamics to a given type of interaction, even as an effective one. In spin systems, there are short-range as well as long-range, isotropic or anisotropic, interactions. These are mostly exchange interactions (EI), dipole-dipole interactions (DDI), or Dzyalozhinski-Moriya interactions (DMI).

On the atomic level, for instance, these three interactions are the most relevant spin-spin interactions and studying them in a systematic way is necessary in order to understand how a local spin excitation would propagate through the magnetic media as it is conveyed by each of these interactions. In particular, this is relevant in the pump-probe like experiments where one is interested in the long-range effect of a (local) demagnetization by a laser or any other source of local heating.

Another example of application of the model considered in this work is that of two magnetic layers, each represented by its macroscopic magnetic moment, separated by a nonmagnetic spacer and coupled through the latter by an effective interaction which is either EI, DDI, or DMI. The static and dynamic properties of such multilayers with effective interactions have been studied experimentally and theoretically by many groups, see e.g., Refs. 4–6 where ultrathin multilayers were studied by the Brillouin Light Scattering technique and the effective coupling was estimated. This model can also be adapted to a pair of macroscopic moments representing two nanoparticles, embedded in a nonmagnetic matrix. Furthermore, this somewhat toy problem may serve as a benchmark for many-particle systems. Moreover, for studying the dynamics of interacting systems one has to understand the dynamics of the elementary brick of two interacting elements and this can be represented as a magnetic dimer (MD).

One of the questions that we address here is how each of these interactions affects the dynamics and, in particular, the magnetization reversal of the MD. For this we first (semi)-analytically compute the switching rates in several situations. Knowing the switching time a comparison with *e.g.* Network Analyzer-Ferromagnetic Resonance(NA-FMR) measurements, should help us to tell which interaction is most rel-

evant in the system studied.

In the absence of thermal fluctuations, the switching is entirely deterministic and occurs at some critical value of the effective field, at which the (effective) energy barrier vanishes. In the case of DDI the switching dynamics has been studied in the past by many authors, see for instance Refs.[7,8]. For classical systems, thermal effects on the dynamics of an MD can be accounted for within the Langevin approach by solving the system of two coupled Landau-Lifshitz equations, one for each magnetic moment, where the effective deterministic field is augmented by the (random) Langevin field[9]. The equivalent approach that consists in solving the corresponding Fokker-Planck equation (FPE) can also be used[10]. In the case of high-to-intermediate damping regime and high-energy barriers, analytical expressions have been obtained for the exchange-coupled MD[11] using Langer's approach[12] and the results have been favorably compared with the numerical approach based on the solution of FPE[13]. In Ref.[11] it was shown that there exists a critical exchange coupling below which the MD reverses its direction via a two-step process, *i.e.* through a fanning mode, whereas above this critical coupling the system switches through a coherent mode. At the critical coupling, some saddle points become flat and Langer's approach, based on the quadratic expansion of the energy, ceases to be valid. As a consequence, the switching rate presents two disconnected branches corresponding to the weak and strong coupling regimes. In Ref.[13] the FPE is transformed into an eigenvalue problem and the latter is then solved using the numerical technique of matrix-continued fractions. This work renders a smooth switching rate for exchange coupling strengths that compares very well with the analytical asymptotes outside the critical region. Finally, it is worth mentioning the work of Solomon[14] where switching processes were studied and the longitudinal and transverse switching times were computed for a quantum MD at room temperature.

In the present work, we use Langer's approach to investigate the dynamics of an MD with three different couplings, EI, DDI, and DMI. The objective here is to compare the dynamics and switching modes in each case with the aim to provide an answer as to which coupling is the most efficient as far as the full switching of the MD is concerned and which configuration is the most optimal for applications. To accomplish this, we consider two orientations of the two anisotropy axes with respect to the bond axis, namely the longitudinal (LA) and transverse (TA) anisotropies. These two anisotropy configurations mimic the two cases of magnetic films with two limiting thicknesses. In order to carry the full analytical calculation of the various switching rates and provide (approximate) sensible analytical expressions thereof, the applied magnetic field has been ignored in this work. The other reason for this restriction is the need to investigate the three couplings and compare the dynamical behavior they entail without the influence of the applied magnetic field. In a subsequent work we intend to include, within a numerical approach, the latter and consider more general configurations of the anisotropy axes.

The paper is organized as follows. In the next section we write all the contributions to the MD energy, introduce our notation, and present the method for computing the various switching rates. In the next section, we deal with the three types of interactions. We first summarize the previous results for an EI-MD and then deal with DDI and DMI, successively. We treat the three cases of i) longitudinal anisotropy (LA) where both anisotropy axes are parallel to the MD bond, ii) transverse anisotropy (TA), with the anisotropies perpendicular to the bond direction, and iii) mixed anisotropy (MA) with one anisotropy axis parallel and the other perpendicular to the bond. In each case we investigate the various coupling regimes and compute the corresponding switching rates. The next section is devoted to a case study of a comparison between the three interactions.

II. ENERGY AND SWITCHING RATE

In this section we define our notations and provide the basic formulae of our calculations, including the energy and the switching rate. For the latter we briefly summarize Langer's kinetic theory that will be used in the case of intermediate-to-high damping (IHD) regime.

A. Energy

As mentioned in the introduction, the system we study consists of two macroscopic magnetic moments $\mathbf{m}_i, i = 1, 2$, which may represent two magnetic layers or two magnetic nanoparticles or still two atomic moments. Each magnetic moment has an effective uniaxial anisotropy that is assumed to result from magneto-crystalline and/or shape anisotropy. In the case of multi-layered systems, we consider both in-plane and out-of-plane anisotropy, thus modeling magnetic films with two limiting thicknesses. The two layers are coupled via the nonmagnetic layer by an effective EI, DDI, or DMI and the corresponding dimer will then be referred to as the EI-MD, DDI-MD, or DMI-MD, respectively. While exchange coupling is invariant under global rotation of the system, DDI and DMI are anisotropic as they originate from a coupling to the lattice. In particular, the magnetic state induced by DDI depends on the orientation of the vector connecting the magnetic moments, the MD bond. For the DDI-MD, for definiteness, we set the

latter in the z direction and the corresponding verse will be denoted $\mathbf{e}_{12}$, *i.e.*, $\mathbf{e}_{12} = \mathbf{e}_z$. The connecting vector $\mathbf{r}_{12}$ is then written as $\mathbf{r}_{12} = d\mathbf{e}_{12}$ where d is the distance between the centers of mass of the two layers. Since the magnetic layers are assumed to be much thinner than the nonmagnetic spacer, the distance d is approximately the thickness of the latter. The anisotropy axes $\mathbf{e}_i, i = 1, 2$ and the applied field with the verse $\mathbf{e}_h$ are *a priory* in arbitrary directions [see Fig. 1].

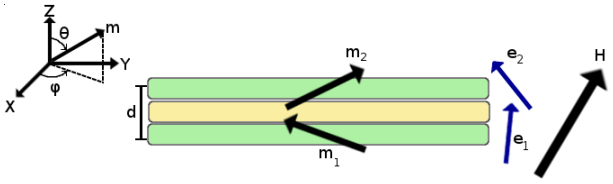

Figure 1: Setup of the DDI-MD with oblique magnetic field and arbitrary anisotropy axes.

In the sequel, we will use spherical coordinates for all vectors involved. Hence, for the magnetic moments we write $\mathbf{m}_i = m_i\,\mathbf{s}_i$, with $\|\mathbf{s}_i\| = 1$ and $\mathbf{s}_i(\theta_i, \varphi_i), i = 1, 2$. The applied field is written $\mathbf{H} = H\,\mathbf{e}_h$, with $\|\mathbf{e}_h\| = 1$ and $\mathbf{e}_h(\theta_h, \varphi_h)$, and the anisotropy axes are $\mathbf{e}_i(\theta_i^{(a)}, \varphi_i^{(a)})$. θ and ϕ are respectively the polar and azimuthal angles as defined in Fig. 1. Note also that the applied field H is to be understood as $\mu_0 H$ which is counted in Tesla.

The energy of the MD then reads

$$E \;=\; E_{\rm Z} + E_{\rm A} + E_{\rm Int} \tag{1}$$

where $E_{\rm Z}$ is the Zeeman energy

$$E_{\rm Z} = -\mathbf{H}\cdot\sum_{i=1,2}\mathbf{m}_i = -\sum_{i=1,2} m_i\,(\mathbf{H}\cdot\mathbf{s}_i)\,, \tag{2}$$

$E_{\rm A}$ is the (uniaxial) anisotropy contribution

$$E_{\rm A} = -\sum_{i=1,2} K_i V_i\,(\mathbf{s}_i\cdot\mathbf{e}_i)^2\,. \tag{3}$$

The interaction energy $E_{\rm Int}$ may stem from the exchange (ferromagnetic) coupling

$$E_{\rm Int} = E_{\rm Exch} = -J\,\mathbf{s}_1\cdot\mathbf{s}_2, \tag{4}$$

from the DM coupling

$$E_{\rm Int} = E_{\rm DM} = -\mathbf{D}\cdot(\mathbf{s}_1\times\mathbf{s}_2)\,, \tag{5}$$

or from the DDI contribution

$$E_{\rm Int} = E_{\rm DDI} = \left(\frac{\mu_0}{4\pi}\right)\left(\frac{m_1 m_2}{d^3}\right)\mathbf{s}_1\cdot\mathcal{D}_{12}\mathbf{s}_2 \tag{6}$$

with

$$\mathcal{D}_{12} \equiv 3\,(\leftarrow\cdot\mathbf{e}_z\mathbf{e}_z\cdot\rightarrow) - 1. \tag{7}$$

being the DDI tensor.

Let's recall that DMI is an anti-symmetrical exchange interaction coming from a combination of low symmetry and spin-orbit coupling[15,16]. In the presence of disorder, especially at the interface of thin films or multilayers, the DMI has been shown to play an important role since local symmetry is broken by surface effects. Indeed, it leads to large anisotropy and may even change the magnetic order, see Ref.[17] and references therein. In particular, it has been shown that DMI is induced by spin-orbit coupling between two ferromagnetic layers separated by a paramagnetic layer[18]. Accordingly, in the present study, it is also relevant to investigate its effect on the dynamics of the MD, on the same footing as the (symmetrical) effective exchange coupling.

Investigating the general situation with arbitrary orientations for the easy axes is rather involved and can only be dealt with numerically. This will be done in a subsequent work. In the present work, we choose to focus on the qualitative behavior of the various interactions and investigate how they affect the dynamics of the system. For this purpose, we consider a situation that can be dealt with analytically, thus allowing for a simpler analysis of the underlying physics. More precisely, we assume equal magnitudes for the two magnetic moments with equal anisotropies (in direction and magnitude), *i.e.* $\mathbf{e}_1 \parallel \mathbf{e}_2$ and $K_1 = K_2$; no external magnetic field.

In the sequel, we will measure the energy in units of the anisotropy energy and thus write

$$\mathcal{E} \equiv \frac{E}{k_B T} = \sigma\frac{E}{KV}$$

where

$$\sigma \equiv \frac{KV}{k_{\rm B}T}$$

is the reduced anisotropy energy and also the reduced energy barrier in the non-interacting case. Therefore, the MD energy reads [the Greek indexes run over x, y, z while the Roman indexes run over $1, 2$]

$$\mathcal{E} = \frac{E}{k_B T} \;=\; \sigma\left[-2h\sum_{\alpha} e_{h,\alpha}\sum_{i=1,2} s_{i,\alpha} - \sum_{i=1,2}\sum_{\alpha,\beta} e_{i,\alpha}e_{i,\beta}s_{i,\alpha}s_{i,\beta}\right] + \mathcal{E}_{\rm Int} \tag{8}$$

with

$$\mathcal{E}_{\rm Int} = -\sigma\sum_{\alpha,\beta} s_{1,\alpha}\left[j\,\delta_{\alpha\beta} + \delta\sum_{\gamma}\varepsilon^{\alpha\beta\gamma}e_{d,\gamma} - \xi\,\mathcal{D}_{12}^{\alpha\beta}\right]s_{2,\beta}. \tag{9}$$

$\varepsilon^{\alpha\beta\gamma}$ is the fully antisymmetric Levi-Civita tensor of rank 3 and $\mathbf{e}_d$ is the verse of $\mathbf{D}$. We have introduced also the following (dimensionless) parameters

$$h \equiv \frac{Hm}{2KV}, \quad j \equiv \frac{J}{KV},$$
$$\delta \equiv \frac{D}{KV}, \quad \xi \equiv \left(\frac{\mu_0}{4\pi}\right)\left(\frac{m^2/d^3}{KV}\right) \tag{10}$$

which imply that all energies are measured in units of the anisotropy energy. For instance, h is the usual ratio of the magnetic field H to the anisotropy field

$$H_A = \frac{2KV}{m} = \frac{2K}{M_s} = \frac{2K_a}{\mu_a}. \tag{11}$$

B. Relaxation rate

It was shown in Refs.[11] that Langer's expression[12] for the escape rate from the minimum $(\theta^{(m)}, \varphi^{(m)})$ through the saddle point $(\theta^{(s)}, \varphi^{(s)})$ takes the more compact form

$$\Gamma = \frac{|\kappa|}{2\pi}\frac{\tilde{Z}_s}{Z_m}, \tag{12}$$

where Z_m and Z_s are respectively the partition functions computed in the vicinity of the minimum and the saddle point and $|\kappa|$ is the attempt frequency. The latter represents the growth rate of a nucleating fluctuation at the saddle point and thus characterizes the unstable barrier-crossing mode. This expression indicates that the escape rate is simply given by the ratio of the total current through the saddle point to the number of particles (or points in the system phase space) in the metastable state. In fact, within Langer's approach the problem of calculating the switching rate for a multi-dimensional process is reduced to solving a steady-state Fokker-Planck equation for the probability density ρ, *i.e.*, $\partial_t \rho = 0$, in the immediate neighborhood of the saddle point that the system crosses as it goes from a metastable state to another state of greater stability. The probability density ρ is connected to the probability current via the continuity equation. On the other hand, ρ can be written as $\rho_{\text{eq}} = e^{-\beta\mathcal{H}}/Z$ times some other function. From these two relations one can write the probability current in terms of the partition function[19,20], see also Ref. 21 for great details. Now, since the switching rate is given by the total probability flux through a surface near the saddle point, Langer's result for the escape rate can be achieved by computing the energy-Hessian eigenvalues near the saddle points and metastable states. From the latter, one then infers the partition function $\tilde{Z}_s$ of the system restricted to the region around the saddle point and the partition function Z_m of the region around the metastable state. When computing these partition functions, one has to identify and take care of each Goldstone mode, that is a massless mode or zero-energy fluctuation associated with a continuous unbroken global symmetry. The tilde on Z_s reminds us of the fact that the negative eigenvalue of the energy Hessian corresponding to the escape route is (formally) taken with the absolute value[23]. Z_s is the product of contributions from all eigenvalues.

In Langer's approach the attempt frequency κ is computed by linearizing the Landau-Lifshitz equation around the saddle point, diagonalizing the resulting transition matrix[21,22], and selecting its negative eigenvalue. However, only in a few situations can κ be obtained analytically. In fact, in the general situation, κ can only be computed numerically. Accordingly, one computes the unique[24] negative eigenvalue κ of the steady-state FPE corresponding to the unstable mode at the saddle point as the negative eigenvalue of the dynamic matrix $\tilde{M}_{mn} = -\lambda_n (PMP^T)_{mn}$, where λ_n are the eigenvalues of the energy Hessian at the saddle point, M the dynamic matrix, and P is the transformation matrix from the initial coordinates to the "canonical" ones.

Therefore, for a given elementary process, *i.e.*, an escape from the minimum $(\theta^{(m)}, \varphi^{(m)})$ through the saddle point $(\theta^{(s)}, \varphi^{(s)})$, we have to compute the partition function

$$Z = \int (\mathcal{D}\mathbf{s})\; e^{-\beta E(\mathbf{s})}$$

at the saddle and metastable states. For this, we perform a quadratic expansion of the energy at these stationary states. This is where Langer's approach meets its limit of validity because such an expansion is only meaningful when the stationary point is well defined. More precisely, Langer's approach is only valid in the case of high energy barriers ΔE, *i.e.*, when $\beta\Delta E \gg 1$ and also intermediate-to-high damping[20,21].

In the case of a two-body problem, such as that of MD, in the weak coupling regime the magnetization of the whole system switches in a two-step process; an example is shown in Fig. 2 in the case of EI-MD. The first step of switching corresponds to the passage of the first magnetic moment from the initial state into an intermediate state through the saddle point. This step lasts the (switching) time τ_1. The second step is taken by the second magnetic moment that then proceeds to switch through a second saddle point and this step lasts the time τ_2. The total time required by the MD to switch is then $\tau = \tau_1 + \tau_2$, and in terms of the switching rate ($\Gamma = \tau^{-1}$), one has

$$\frac{1}{\Gamma} = \frac{1}{\Gamma_1} + \frac{1}{\Gamma_2}.$$

Next, for fully identical magnetic moments one has to consider the left-right symmetry and multiply the expression above by a factor of 2 leading to the final

expression for the switching rate corresponding to the two-step process of the MD

$$\Gamma_{\rm total} = 2\frac{\Gamma_1\Gamma_2}{\Gamma_1+\Gamma_2}. \tag{13}$$

In fact, one may have other symmetry factors depending on the system setup.

Consequently, in the sequel our task will consist in analyzing the energy potential surface in each situation, studying the various switching paths, and combining the corresponding switching rates according to Eq. (13). For each elementary step corresponding to an escape from a minimum through a saddle point we will use Eq. (12) to compute the corresponding switching rate.

Defining the characteristic time of the underlying material $t_s = (\gamma H_A)^{-1} = \mu_a/(2\gamma K_a)$, where $\gamma \simeq 1.76\times10^{11}$ (T.s)$^{-1}$ is the gyromagnetic factor, the final (dimensionless) switching rate may be given in s^{-1} upon multiplying by

$$\frac{\gamma k_B T}{\mu_a} = \frac{1}{2}\left(\frac{2\gamma KV}{\mu_s}\right)\left(\frac{k_BT}{KV}\right) = \frac{1}{2}\frac{t_s^{-1}}{\sigma}. \tag{14}$$

For cobalt, for instance, we have $\mu_a = 1.57\times10^{-23}Am^{-1}atom^{-1}$, $K_a = 2.53\times10^{-24}Jatom^{-1}$, leading to $t_s = 1.76\times10^{-11}s$.

In this work we compute the relaxation rate by combining Langer's approach, which is valid in the IHD regime, and the Landau-Lifshitz equation (LLE) with its phenomenological damping parameter. Using the LLE for obtaining the attempt frequency in the prefactor in Eq. (12) leads to spurious effects when one formally takes the limits $\alpha \to 0$ or $\alpha \to \infty$.[25] However, Langer's expression for the relaxation rate may be "regularised" by using Gilbert's damping instead of the Landau-Lifshitz damping. Indeed, the latter may be shown to be identical to Gilbert's if the gyromagnetic factor γ is replaced by $\gamma^* = \gamma/\left(1+\alpha^2\right)$. In the present calculations this amounts to replacing the scaling time t_s defined above by $t_s^* = t_s\left(1+\alpha^2\right)$. In fact, Landau-Lifshitz and Gilbert's equations are related by the transformation

$$\gamma \to \frac{\gamma}{1+\alpha^2}, \qquad \alpha \to \frac{\alpha}{1+\alpha^2}.$$

We recall that our main objectives in this work are: i) an investigation of the behaviour of the relaxation rate as a function of the MD coupling and ii) a pairwise comparison of three types of layer coupling (exchange, dipolar, and Dzyaloshiski-Moriya). In particular, we do not investigate the damping dependence of the relaxation rate. A thorough study of all crossovers between the various damping regimes is given in Ref. 20 where one can see that the boundaries between the regimes are not simply $\alpha = 1$.

III. EXCHANGE COUPLED MAGNETIC DIMER

In this section, for later use, we briefly summarize the results of Ref.[11]. The situation is sketched in Fig. 2.

In the case of parallel easy axes and longitudinal field, it was found that there is a critical exchange coupling j_c that depends on the applied field and anisotropy constant, *i.e.* $j_c(H,K)$, above which the MD behaves as a macrospin with a double energy barrier that switches from a metastable state to a more stable one in a coherent manner, see Fig. 2 (right). Below j_c the system is weakly coupled and switches in a two-step process through two different escape routes (saddle points), see Fig. 2 (left). Setting $\mathbf{e}_h \parallel \mathbf{e}_1 \parallel \mathbf{e}_2$, in the notations of Eq. (10), the critical exchange coupling j_c was found to be

$$j_c = 1 - h^2. \tag{15}$$

For $j > j_c$, the MD switches from the metastable state (π,π,φ), that is a ferromagnet, against the field, into the ferromagnetic state $(0,0,\varphi)$, through the saddle point $(\arccos(-h), \arccos(-h), \varphi)$. The angle φ is arbitrary because of the uniaxial symmetry and the equality of the spin polar angles is due to the fact that the two spins are identical (same amplitude and same anisotropy). The corresponding switching rate is given by (in zero field)

$$\Gamma_{j>j_c} = \alpha\sqrt{\frac{2\sigma}{\pi}}\frac{1+1/j}{\sqrt{1-1/j}}e^{-\sigma}. \tag{16}$$

In the weak-coupling regime $j < j_c$, the switching rate is obtained by combining the switching rates corresponding to the two escape routes taken by the two spins, see Fig. 2 (left). The result is somewhat more involved and given in Refs.[11], see also Ref.[13].

The escape rate for the EI-coupled MD will be compared to the other two cases of DDI- and DMI-coupled MD. For this purpose, we recall here the energy barriers (in the absence of the magnetic field)

$$\Delta\mathcal{E} = \frac{\sigma}{2}(1\pm j). \tag{17}$$

IV. DIPOLAR COUPLED MAGNETIC DIMER

We consider both the longitudinal and transverse anisotropies, *i.e.* $\mathbf{e}_1 \parallel \mathbf{e}_2 \parallel \mathbf{e}_{12} \parallel \mathbf{e}_z$ and $\mathbf{e}_1 \parallel \mathbf{e}_2 \perp \mathbf{e}_{12} \parallel \mathbf{e}_z$, respectively, which will be referred to as the LA and TA setup, respectively. Furthermore, we will also discuss the case of mixed anisotropy, $\mathbf{e}_1 \parallel \mathbf{e}_{12}, \mathbf{e}_2 \perp \mathbf{e}_{12}$, which would mimic the case of an MD with a sufficiently thin film coupled to a sufficiently thick one. Comparison with the exchange-coupled MD will be done only in the case of LA, considered in Refs.[11].

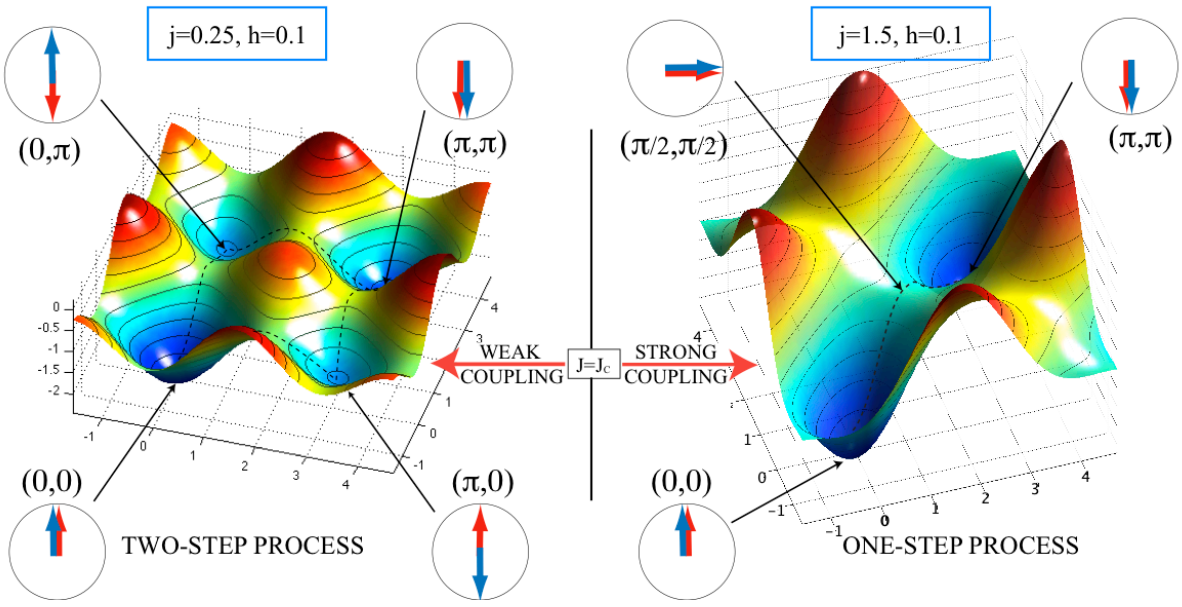

Figure 2: Crossover from a two-step to a one-step switching to its stable state (SS) of an EI-MD with LA.

A few general assumptions allow us to simplify the problem without any loss of generality as far as the underlying physics is concerned. Indeed, in the sequel, we will assume the following. If there is no magnetic field, the equilibrium orientation of the net magnetic moment is in the plane defined by the DDI axis and the anisotropy axes. The latter are assumed to lie in the xz plane, *i.e.*, $\varphi_1^{(a)} = \varphi_2^{(a)} = 0$. Consequently, the energy becomes

$$\begin{aligned} \mathcal{E} &= -\sigma \sum_{i=1,2} \cos^2\left(\theta_i - \theta_i^{(a)}\right) \\ &\quad -\sigma\xi\left[2\cos\theta_1\cos\theta_2 - \sin\theta_1\sin\theta_2\cos\left(\varphi_1-\varphi_2\right)\right]. \end{aligned} \tag{18}$$

The analytical study will be further restricted to the following three cases:

1. Longitudinal anisotropy (LA): both anisotropy axes are parallel to the MD axis $\mathbf{e}_{12}$, *i.e.* $\theta_1^{(a)} = 0 = \theta_2^{(a)}$. Moreover, due to the fact that all contributing fields are acting in the same plane, the two magnetic moments of the MD will move in the same plane so that $\varphi_1 = \varphi_2$.
2. Transverse anisotropy (TA): both anisotropy axes are perpendicular to the MD axis, $\theta_1^{(a)} = \frac{\pi}{2} = \theta_2^{(a)}$.
3. Mixed anisotropy (MA): one anisotropy axis is parallel to the MD axis and the other perpendicular to it, $\theta_1^{(a)} = 0, \theta_2^{(a)} = \frac{\pi}{2}$.

Differentiating with respect to the remaining variables, *i.e.* the two polar angles $\theta_i, i = 1, 2$, leads to the various equations for the stationary states whose solutions depend on the anisotropy setup.

A. Longitudinal anisotropy

The whole set of stationary states is given by

$$\begin{aligned} (\theta_1,\theta_2) &= (0,\pm\pi),(\pm\pi,0),(\pm\pi,\pm\pi),(\pm\pi,\mp\pi), \\ &\left(\pm\frac{\pi}{2},\pm\frac{\pi}{2}\right),\left(\pm\frac{\pi}{2},\mp\frac{\pi}{2}\right) \end{aligned}$$

together with the following ones (which are saddle points) for $\xi \leq \frac{2}{3}$ or $\xi \geq 2$,

$$(\cos\theta_1,\cos\theta_2) = (\pm x_1^\epsilon, \pm x_2^\epsilon),(\pm x_1^\epsilon, \mp x_2^\epsilon) \tag{19}$$

where

$$\begin{aligned} x_1^\epsilon &= \frac{1}{\sqrt{2}}\sqrt{1+\frac{3}{4}\xi^2 - a^\epsilon}, \qquad x_2^\pm = x_1^\mp \\ a^\epsilon &\equiv \epsilon\sqrt{\left(\frac{\xi^2}{4}-1\right)\left(9\frac{\xi^2}{4}-1\right)} \equiv \epsilon a, \quad \epsilon = \pm. \end{aligned} \tag{20}$$

It can be checked that the radicant is always positive and no additional special ranges are found regarding the existence of the roots. However, as x_1^ϵ and x_2^ϵ are cosines they must satisfy $-1 \leq x_i^\epsilon \leq 1$, which is only true for $\xi \leq \frac{2}{3}$. Hence we can identify two different regimes, the weak-coupling (WC) regime $\xi \leq \frac{2}{3}$, and the strong-coupling (SC) regime $\xi \geq \frac{2}{3}$. We will see later that this critical value corresponds to the vanishing of the smallest eigenvalue of the energy Hessian at one of the energy minima. It also marks

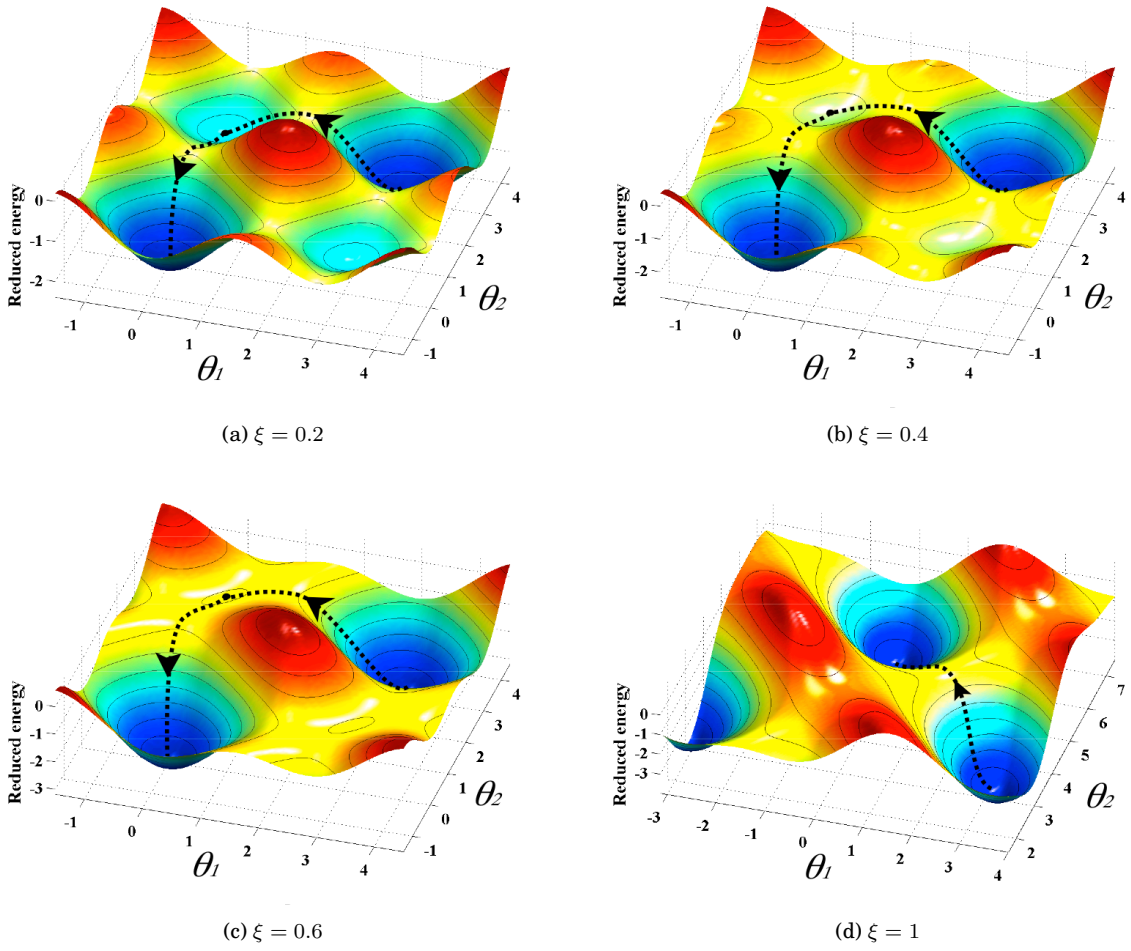

(a) $\xi = 0.2$ (b) $\xi = 0.4$

(c) $\xi = 0.6$ (d) $\xi = 1$

Figure 3: Evolution of the energy potential surface of a DDI-MD with longitudinal anisotropy configuration as ξ increases, with $\sigma = 1.5$.

the nucleation of a particular switching mode and allows us to determine the nucleation field[7,8].

The energy potential surface for this situation is shown in Fig. 3 for a varying DDI strength ξ.

1. *Weak coupling ($\xi \leq \frac{2}{3}$)*

The minima correspond to ferromagnetic (FM) states along the DDI axis

$$(\theta_1, \theta_2) = (0, 0), (\pi, \pi). \tag{21}$$

The metastable states are the anti-ferromagnetic (AFM) states along the DDI axis

$$(\theta_1, \theta_2) = (0, \pi), (\pi, 0) \tag{22}$$

and the maxima are the (anti)ferromagnetic states perpendicular to the DDI axis

$$(\theta_1, \theta_2) = \left(\pm\frac{\pi}{2}, \pm\frac{\pi}{2}\right), \left(\pm\frac{\pi}{2}, \mp\frac{\pi}{2}\right). \tag{23}$$

Finally, the saddle points are located at

$$(\theta_1, \theta_2) = (\varepsilon_1 \arccos(\varepsilon_2 x_1^{\gamma}), \varepsilon_1 \arccos(\varepsilon_2 x_2^{\gamma})) \tag{24}$$

where the signs $\varepsilon_1 = \pm$ and $\varepsilon_2 = \mp$ are independent of each other.

Now we compute the switching rate in this coupling regime. In Fig. 3a we see that the system goes through the following steps: i) from the state (π, π) to the state $(0, \pi)$ through the saddle point

$$\left(\cos\theta_1^{(1)} = x_1^{+}, \cos\theta_2^{(1)} = -x_2^{+}\right) \tag{25}$$

[see Eq. (24)], and then ii) it passes from the state $(0, \pi)$ to the state $(0, 0)$ through the saddle point

$$\left(\cos\theta_1^{(2)} = x_1^{-}, \cos\theta_2^{(2)} = -x_2^{-}\right). \tag{26}$$

These transitions are sketched in Fig. 4 (left).

Therefore, in order to compute the switching rate corresponding to the two-step process $(\pi, \pi) \rightarrow$

$(0,\pi) \to (0,0)$ we need to compute the switching rate of each step and combine them according to the rule in Eq. (13) where the individual switching rates are then computed using Langer's expression (12).

In order to compute the switching rate $\Gamma_{(\pi,\pi)\to(0,\pi)}$ we first compute the partition function at the minimum (π,π) and at the saddle point $\left(\theta_1^{(1)},\theta_2^{(1)}\right)$, namely

$$Z_{(\pi,\pi)} \simeq \frac{(2\pi)^2}{\sigma^2\,(2+3\xi)\,(2+\xi)} e^{2\sigma(1+\xi)}. \tag{27}$$

Likewise, the partition function at the metastable state $(0,\pi)$ is

$$Z_{(0,\pi)} = \frac{(2\pi)^2}{\sigma^2\,(2-\xi)\,(2-3\xi)} e^{2\sigma(1-\xi)}. \tag{28}$$

This result can also be found upon noting that since the anisotropy is uniaxial, in order to change the system minimum from the ferromagnetic state (π,π) to the anti-ferromagnetic state $(0,\pi)$, we can simply change the sign of the interaction, *i.e.* replace ξ by $-\xi$.

The lowest eigenvalue of the energy Hessian at the metastable minimum is $\lambda = \sigma\,(2-3\xi)$. As mentioned earlier, we see that when this eigenvalue vanishes it yields the critical value for the DDI coupling, namely $\xi = 2/3$. Indeed, the nucleation field in this case is $h_n \propto \sigma\,(2-3\xi)$ which coincides with the result of Refs. 7,8,10. In Ref. 10 the authors defined the parameter for the DDI strength $k_{\rm int}$ as the ratio of the DDI field to the anisotropy field. In our notations, $k_{\rm int} = \xi/2$. The critical value of $k_{\rm int} = 1/3$ coincides with our condition $\xi = 2/3$.

At the saddle point (25) the energy is

$$\mathcal{E}_0^{(1)} \;=\; \sigma\left(\frac{3}{4}\xi^2 - 1\right) \tag{29}$$

and the energy barrier separating the minimum (π,π) from the saddle point $\left(\theta_1^{(1)},\theta_2^{(1)}\right)$ is

$$\Delta\mathcal{E}^{(1)} = \sigma\left(1 + 2\xi + \frac{3}{4}\xi^2\right). \tag{30}$$

This is plotted in Fig. 5 where we see that the (weak) DDI brings a correction $\sigma\left(2\xi + \frac{3}{4}\xi^2\right)$ to the free MD energy barrier $\Delta\varepsilon = \sigma$. For ferromagnetic order ($\xi > 0$), this correction enhances the energy barrier and this is compatible with the fact that due to the ferromagnetic coupling, it is more difficult for the first spin to switch.

Within Langer's approach to the calculation of the switching rate the saddle point may retain a subgroup of the symmetry group of the system, in which case some of the Hessian eigenvalues at the saddle point vanish, and then a special treatment is required for this situation. For the one-spin problem with uniaxial anisotropy, for instance, the saddle point has a $U(1)$ symmetry around the z axis, or with respect to the rotation $\mathcal{R}\,(\mathbf{e}_z,\varphi)$. This leads to a vanishing eigenvalue of the Hessian at the saddle point corresponding to fluctuations with respect to the angle φ ($\simeq \varphi^s + p$), where φ^s is the value of the azimuthal angle at the saddle point. Likewise, the saddle points (25, 26) have rotational symmetry with respect to the azimuthal angle and as such one should use the energy

$$\begin{aligned}\mathcal{E} \;&=\; -\sigma\left[\cos^2\theta_1 + \cos^2\theta_2\right] \\ &\quad -\sigma\xi\left[2\cos\theta_1\cos\theta_2 - \sin\theta_1\sin\theta_2\cos\varphi\right]\end{aligned}$$

where $\varphi \equiv \varphi_1 - \varphi_2$. The saddle points (25, 26) should refer both to the polar angles θ_i and to a given value of the azimuthal angle φ, even if it is arbitrary.

Let us then perform the expansion around the saddle point $\left(\theta_i^{(s)},\varphi_i^{(s)}\right)$

$$t_i = \theta_i - \theta_i^{(s)}, p_i = \varphi_i - \varphi_i^{(s)},\; i = 1,2$$

and expand the energy above to second order in the small variables t_i, p_i. Doing so we obtain

$$\begin{aligned}\mathcal{E}^{(1)} \;&\simeq\; \mathcal{E}_0^{(1)} + 2\sigma\,(t_1,t_2)\begin{pmatrix} a & 0 \\ 0 & -a\end{pmatrix}\begin{pmatrix} t_1 \\ t_2\end{pmatrix} \\ &\quad +\frac{\sigma}{2}\,(\pi_+,\pi_-)\begin{pmatrix} 0 & 0 \\ 0 & \xi^2\end{pmatrix}\begin{pmatrix} \pi_+ \\ \pi_-\end{pmatrix}\end{aligned}$$

where $\pi_\pm = \dfrac{p_1 \pm p_2}{\sqrt{2}}$.

Note that the mode corresponding to π_+ is a soft mode, *i.e.*, a zero-energy mode, or still a Goldstone mode. This corresponds to the $U\,(1)$ symmetry mentioned earlier and that must be dealt with properly in order to avoid the divergence of the partition function. In fact, integration over this variable simply yields the factor 2π. The partition function is then given by

$$\tilde{Z}_s^{(1)} = \sqrt{2}\left(\frac{\pi}{\sigma}\right)^{5/2}\frac{\sigma}{a}e^{-\mathcal{E}_0^{(1)}}. \tag{31}$$

Hence, gathering the results in Eqs. (27) and (31) into the first equation of (12), we obtain

$$\Gamma_{(\pi,\pi)\to(0,\pi)} \;=\; \left|\kappa^{(1)}\right|\sqrt{\frac{\sigma}{2\pi}}\frac{(2+3\xi)\,(2+\xi)}{2a}e^{-\Delta\mathcal{E}^{(1)}}.$$

At the second saddle point (26) the energy is the same, i.e.,

$$\mathcal{E}_0^{(2)} \;=\; \sigma\left(\frac{3}{4}\xi^2 - 1\right)$$

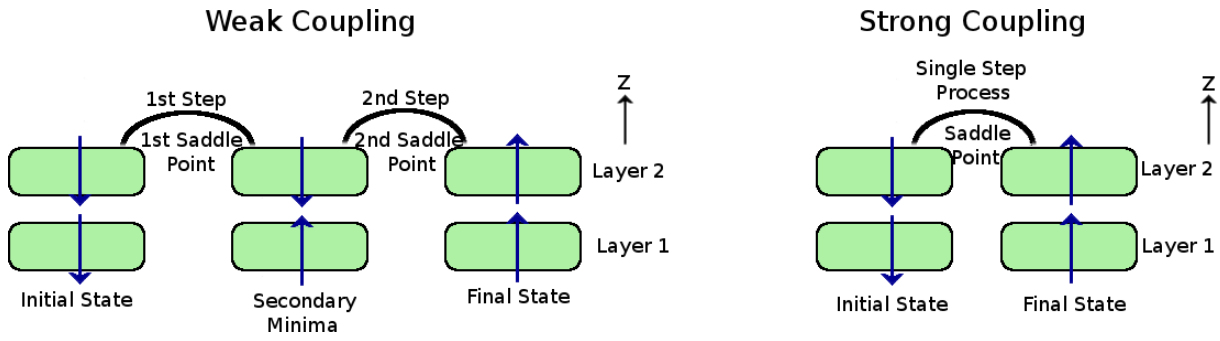

Figure 4: Escape route of the MD with LA.

whereas the energy barrier separating the minimum $(0,\pi)$ from the saddle point $(\theta_1^{(2)},\theta_2^{(2)})$ reads

$$\Delta\mathcal{E}^{(2)} \;=\; \sigma\left(1-2\xi+\frac{3}{4}\xi^2\right). \tag{32}$$

Here the correction to the energy barrier of the free MD starts with a negative coefficient which implies that this energy barrier decreases when ξ increases, see Fig 5. Indeed, as the DDI becomes stronger, the first moment, which has already switched, exerts a stronger force on the first moment. On the opposite, the second energy barrier (30) increases with ξ. When the system is in the initial ferromagnetic state (π,π), it is much more difficult for the first magnetic moment to break free from the ferromagnetic coupling.

The corresponding switching rate then reads

$$\Gamma_{(0,\pi)\to(0,0)} \;=\; \left|\kappa^{(2)}\right|\sqrt{\frac{\sigma}{2\pi}}\frac{(2-3\xi)\,(2-\xi)}{2a}e^{-\Delta\mathcal{E}^{(2)}}.$$

Note that we have the symmetry $\Gamma_{(0,\pi)\to(0,0)} = \Gamma_{(\pi,\pi)\to(0,\pi)}\,(\xi\longrightarrow-\xi)$. In both switching rates the prefactor κ has been computed numerically. The total switching rate of the MD is obtained upon using Eq. (13) and is plotted in Fig. 6.

2. *Strong coupling ($\xi \geq 2/3$)*

The situation now is sketched in Fig. 4 (right) with the minima

$$(\theta_1,\theta_2) = (0,0)\,,(\pi,\pi)\,, \tag{33}$$

maxima

$$(\theta_1,\theta_2) = \left(\pm\frac{\pi}{2},\pm\frac{\pi}{2}\right), \tag{34}$$

and saddle points

$$(\theta_1,\theta_2) = \left(\pm\frac{\pi}{2},\mp\frac{\pi}{2}\right). \tag{35}$$

Comparing with the WC regime, we note that the global minima remain the same, while the metastable minima and the saddle points are no longer stationary states. On the other hand, the anti-ferromagnetic states given by $\left(\pm\frac{\pi}{2},\mp\frac{\pi}{2}\right)$ change as well, being maxima for the WC regime they turn into saddle points in the SC regime, creating a switching path in which both magnetic moments switch coherently in a one-step process, as shown in Fig. 4

Following the same procedure as for WC, we obtain the expression for the switching rate in this SC regime of DDI-MD

$$\Gamma_{\mathrm{LASC}} \;=\; \alpha\tilde{\kappa}\sqrt{\frac{\sigma}{\pi}}\,(3\xi+2)\sqrt{\frac{2+\xi}{\xi\,(3\xi-2)}}e^{-\sigma(2+\xi)} \tag{36}$$

where

$$\tilde{\kappa} = \left(1-\frac{\xi}{2}\right)+\sqrt{\left(1+\frac{3}{2}\xi\right)^2+\frac{2}{\alpha^2}\xi\,(2+\xi)}. \tag{37}$$

Fig. 5 shows the evolution of the energy barrier as a function of the DDI coupling ξ. We clearly see the two coupling regimes separated by the critical value $\xi = 2/3$. In the WC regime we do see the two different energy barriers corresponding to the two steps of the reversal process. The energy barrier is continuous for all ξ, including the critical region. Moreover, the second step disappears at $\xi = 2/3$ and the dynamics of the system becomes a one-step process.

Figure 6 shows the behavior of the reduced switching time $\tau = 1/\Gamma = t/2t_s$ as a function of the reduced anisotropy barrier σ for both coupling regimes.

The total switching time may be written as $\tau_{\mathrm{WC}} = \tau_{(\pi,\pi)\to(0,\pi)} + \tau_{(0,\pi)\to(0,0)}$ and it is clear that $\tau_{(\pi,\pi)\to(0,\pi)} \gg \tau_{(0,\pi)\to(0,0)}$ since in the first step one of the magnetic moments has to win against the effective FM coupling. Consequently, as the DDI coupling increases the magnetic moment switching during the first step becomes more and more difficult to

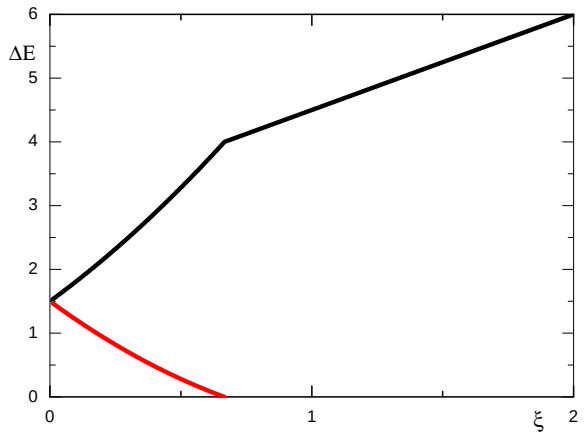

Figure 5: Energy barrier as function of ξ for the LA-MD, with $\sigma = 3/2$.

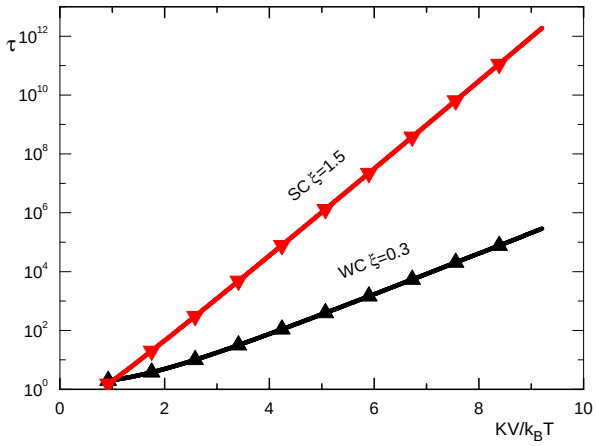

Figure 6: Reduced switching time τ of the DDI-MD with LA as a function of σ for weak and strong coupling regimes .

achieve and thereby the corresponding switching time increases, which explains why $\tau_{\mathrm{LAWC}} < \tau_{\mathrm{LASC}}$.

B. Transverse anisotropy

In spherical coordinates the energy now reads

$$\begin{aligned}\mathcal{E} &= -\sigma\left(\sin^2\theta_1 + \sin^2\theta_2\right) \\ &\quad -\sigma\xi\left[\cos\left(\theta_1+\theta_2\right) + \cos\theta_1\cos\theta_2\right]\end{aligned} \tag{38}$$

In this situation, we find that there are two minima with the corresponding lowest eigenvalues $\sigma\left(2-\xi\right)$ and $\sigma\left(2-3\xi\right)$ whose vanishing leads to the two critical DDI couplings $\xi = 2$ and $\xi = 2/3$.

1. *Weak coupling*($\xi \leq 2/3$)

The absolute minima of the system are now

$$\left(\theta_1,\theta_2\right) = \left(\pm\frac{\pi}{2}, \mp\frac{\pi}{2}\right) \tag{39}$$

while the local minima are given by

$$\left(\theta_1,\theta_2\right) = \left(\pm\frac{\pi}{2}, \pm\frac{\pi}{2}\right). \tag{40}$$

On the other hand, the absolute maxima are the anti-ferromagnetic states

$$\left(\theta_1,\theta_2\right) = \left(0,\pi\right),\left(\pi,0\right) \tag{41}$$

while the local maxima correspond to the ferromagnetic states

$$\left(\theta_1,\theta_2\right) = \left(0,0\right),\left(\pi,\pi\right). \tag{42}$$

Finally, the saddle points are

$$\left(\theta_1,\theta_2\right) = \left(\varepsilon_1\arccos(\varepsilon_2 x_1^{\gamma}), \varepsilon_1\arccos(\varepsilon_2 x_2^{\gamma})\right). \tag{43}$$

The escape route is sketched in Fig. 7 (left).

In the present case, as can be seen in Fig. 8, the initial state is given by $(\frac{\pi}{2}, -\frac{\pi}{2})$, the metastable minimum is $(\frac{\pi}{2}, \frac{\pi}{2})$, and the first and second saddle points are given by $(\arccos x_1^{+}, \arccos x_2^{+})$ and $(\arccos x_1^{-}, \arccos x_2^{-})$, respectively. In this weak coupling regime, the MD switching is again a two-step process and the corresponding switching rates are given by

$$\begin{aligned}\Gamma^{(1)}_{\mathrm{TAWC}} &= \left|\frac{\kappa^{(1)}}{\xi}\right| \frac{1}{2\sqrt{3}\pi a}\sqrt{\left(3\xi+2\right)\left(1+\xi\right)\left(2-\xi\right)} \times e^{-\frac{3\sigma}{2}\left(\frac{2}{3}+\xi\right)\left(1-\frac{\xi}{2}\right)} \\ \Gamma^{(2)}_{\mathrm{TAWC}} &= \Gamma^{(1)}_{\mathrm{TAWC}}\left(\xi \to -\xi\right)\end{aligned} \tag{44}$$

where the attempt frequencies $\kappa^{(i)}, i = 1,2$ are calculated numerically; a is defined in Eq. (20). The total

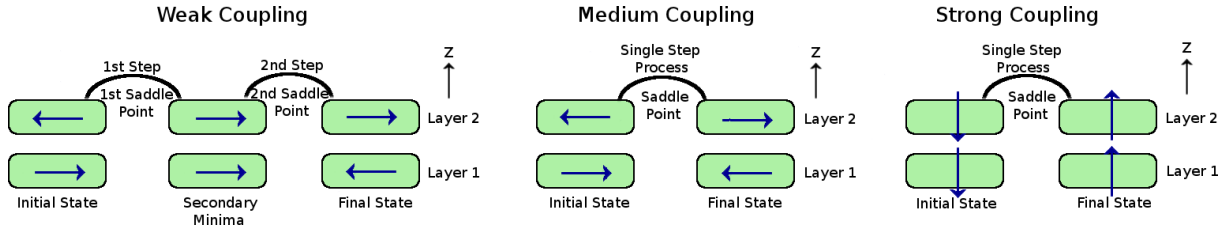

Figure 7: Escape route for the three DDI coupling regimes with TA configuration

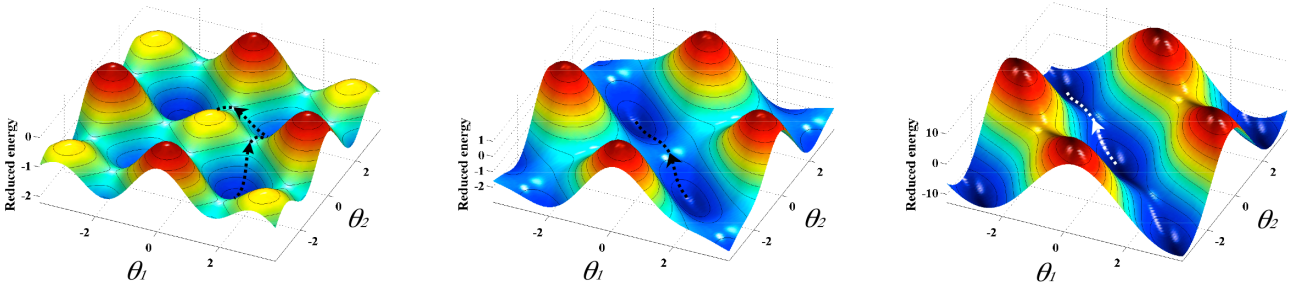

(a) Weak Coupling $\xi = 0.2$ (b) Medium coupling $\xi = 1$ (c) Strong Coupling $\xi = 6.33$

Figure 8: Energy potential surface for the different regimes of the MD with TA and identical $\sigma = 3/2$.

switching rate is given by Eq. (13).

2. *Medium coupling* ($\frac{2}{3} < \xi < 2$)

The minima are given by

$$(\theta_1, \theta_2) = \left(\pm\frac{\pi}{2}, \mp\frac{\pi}{2}\right), \tag{45}$$

the maxima correspond to the anti-ferromagnetic states

$$(\theta_1, \theta_2) = (0, \pi), (\pi, 0), \tag{46}$$

and the saddle points are the ferromagnetic states

$$(\theta_1, \theta_2) = (0, 0), (\pi, \pi) \tag{47}$$

and

$$(\theta_1, \theta_2) = \left(\pm\frac{\pi}{2}, \pm\frac{\pi}{2}\right). \tag{48}$$

Starting from the initial state $(\frac{\pi}{2}, -\frac{\pi}{2})$, the switching is a single-step process in which the two magnetic moments switch coherently through the saddle point $(0, 0)$ leading into the state $(-\frac{\pi}{2}, \frac{\pi}{2})$, as shown in Fig. 7 (middle).

The switching rate for this coupling regime reads

$$\Gamma_{\mathrm{TAMC}} = \frac{\alpha(\xi - 2)}{\pi}\sqrt{\frac{(3\xi + 2)(1 + \xi)}{3\xi^2(3\xi - 2)}}e^{-\sigma(2-\xi)} \tag{49}$$

where the attempt frequency has been obtained analytically and is given by $\kappa = 2\alpha(\xi - 2)$.

3. *Strong coupling* ($\xi > 2$)

Here the DDI field is twice larger than the anisotropy field and the minima are the ferromagnetic states

$$(\theta_1, \theta_2) = (0, 0), (\pi, \pi), \tag{50}$$

the maxima are the anti-ferromagnetic states

$$(\theta_1, \theta_2) = (0, \pi), (\pi, 0), \tag{51}$$

and the saddle points are located at

$$(\theta_1, \theta_2) = \left(\pm\frac{\pi}{2}, \pm\frac{\pi}{2}\right), \left(\pm\frac{\pi}{2}, \mp\frac{\pi}{2}\right). \tag{52}$$

As the DDI coupling increases and the system enters the strong coupling regime, the states that previously were minima in the medium coupling regime become saddle points, and *vice versa*. The system still relaxes in a one step process, but this time from the initial state $(0, 0)$ through the saddle point $(-\frac{\pi}{2}, \frac{\pi}{2})$. This is sketched in Fig.7 (right). The switching rate in this case reads

$$\Gamma_{\mathrm{TASC}} = \frac{|\kappa|}{\pi}\sqrt{\frac{3\xi^2(3\xi - 2)}{(2 + 3\xi)(1 + \xi)}}e^{-\sigma(\xi-2)} \tag{53}$$

with

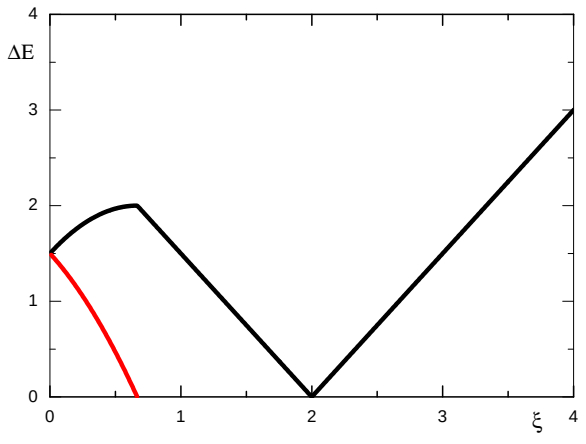

Figure 9: Energy barrier of the MD with TA as a function of ξ, $\sigma = 3$.

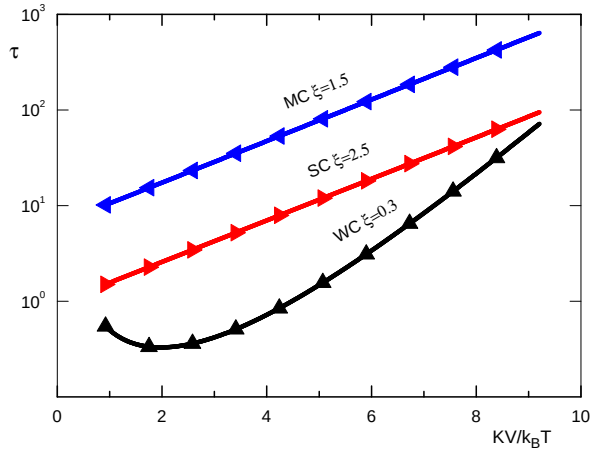

Figure 10: Reduced switching time τ of the MD with TA for the three different coupling regimes as a function of σ.

$$\kappa = \alpha \left[(4+\xi) - \sqrt{9\xi^2 + \frac{8}{\alpha^2}(\xi^2 - \xi - 2)} \right].$$

Fig. 9 shows the evolution of the energy barrier as ξ changes. Similarly to Fig. 5, the different regimes are clearly identified, so are the continuity of the barrier and the disappearance of the second step at $\xi = 2/3$. At $\xi = 2$, we can see that the energy barrier vanishes forming a "furrow" that connects directly (with no energy barriers) the states $(0,0)$, (π,π), and $(\pm\frac{\pi}{2}, \mp\frac{\pi}{2})$. Figure 10 shows the behavior of the switching time in the three regimes of DDI coupling, namely WC, MC and SC; it is a plot of the inverse of the expressions (44), (49), and (53), respectively.

We again observe that the SC switching time is longer than that of the WC, similar to what we have observed in the case of LA, see Fig.6. Furthermore, we see that, as a function of $\sigma \sim 1/T$, the (logarithm of) the switching time in the WC regime is not a straight line. This implies that the prefactor plays a dominant role. As ξ increases the switching time becomes dominated by the Arrhenius (exponential) law where the prefactor is a constant thus leading to a straight line in a logarithmic plot of the switching rate as a function of σ. One of the consequences of a dominant prefactor is that the switching rate becomes quite sensitive to damping and thus to the coupling of the system to its thermal bath and to the various fluctuations.

C. Mixed anisotropy

Whereas the LA and TA configurations for DDI coupling have a somewhat similar behavior in terms of energy potential surface evolution and coupling regimes, the MA shows a completely different and more complex behavior, as can be seen in Fig. 11. Analysis of the stationary states reveals the presence of two coupling regimes as well, but with a critical value now at $\xi = \frac{2}{\sqrt{3}}$. As before, switching in the WC regime is again a two-step process while it is a one-step process in the SC regime. The stationary states are given by Eq. A1 together with

$$\begin{aligned}(\theta_1, \theta_2) \;=\; & (0, \pm\pi), (\pm\pi, 0), (\pm\pi, \pm\pi), \\ & (\pm\pi, \mp\pi), \left(\pm\frac{\pi}{2}, \pm\frac{\pi}{2}\right), \left(\pm\frac{\pi}{2}, \mp\frac{\pi}{2}\right).\end{aligned}$$

It is worth investigating this case because it corresponds to another interesting situation with a rather thick layer coupled to a rather thin layer. It may also be relevant in the situation of a soft magnetic layer coupled to another hard magnetic layer.

The remaining stationary states are rather cumbersome and they are relegated to the appendix.

1. *Weak coupling*($\xi \leq \frac{2}{\sqrt{3}}$)

The individual switching rates are given by Eq. (A2), and the full switching rate is given by Eq. (13). The corresponding analytical expressions are too cumbersome and are thus given in the appendix. They are plotted in Fig. 13. In this case too, κ is computed numerically.

2. *Strong coupling* ($\xi > \frac{2}{\sqrt{3}}$)

The minima now are the FM states

$$(\theta_1, \theta_2) = (0,0), (\pi,\pi)$$

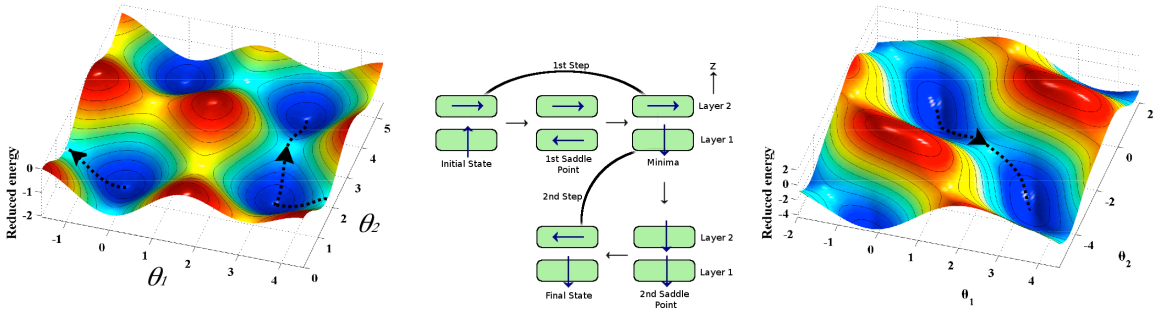

(a) Weak Coupling $\xi = 0.2$ (b) Approximate escape route WC (c) Strong Coupling $\xi = 1.66$

Figure 11: Energy potential surface for the different regimes of the MD and WC escape route with MA and $\sigma = \frac{3}{2}$.

and the maxima are the AFM states

$$(\theta_1, \theta_2) = (0, \pi), (\pi, 0)$$

while the saddle points are

$$(\theta_1, \theta_2) = \left(\pm\frac{\pi}{2}, \pm\frac{\pi}{2}\right), \left(\pm\frac{\pi}{2}, \mp\frac{\pi}{2}\right).$$

Starting in the WC regime, as the DDI coupling increases, the minima given by

$$\left(\pm(\arccos x_+^- - \arccos x_-^-)/2, \pm(\arccos x_+^- + \arccos x_-^-)/2\right)$$

start to merge into the saddle point $(0, 0)$. When the system enters the SC coupling regime, these two minima completely merge leading to the transformation of the state $(0, 0)$ from a saddle point into a minimum. The minima

$$\begin{aligned}(\pm\pi \ &\mp \ (\arccos x_+^- + \arccos x_-^-)/2,\\ \pm\pi \ &\mp \ (\arccos x_+^- - \arccos x_-^-)/2)\end{aligned}$$

have a similar behavior around the state (π, π), while the saddle points $\left(\pm\frac{\pi}{2}, \mp\frac{\pi}{2}\right)$ do not change. The escape route in the SC regime is similar to that of the SC for LA and TA. However, the shape of the energy potential surface presents curved paths instead of the usual straight paths, see Fig. 11.

The escape rate from the initial state $(0, 0)$ through the saddle point $(-\frac{\pi}{2}, \frac{\pi}{2})$ is given by

$$\Gamma_{\text{MASC}} = \frac{|\kappa|}{\pi} e^{-\sigma\xi} \times \sqrt{\frac{\left[(1+2\xi)^2 - r^2\right]\left[4\xi^2 - r_p^2\right]}{\left[(1+\xi)^2 - r^2\right]\left[(\xi + 2r)\,|\xi - 2r|\right]}}, \quad (54)$$

where $r = \sqrt{1+\xi^2}, r_p = \sqrt{4+\xi^2}$. κ is computed numerically.

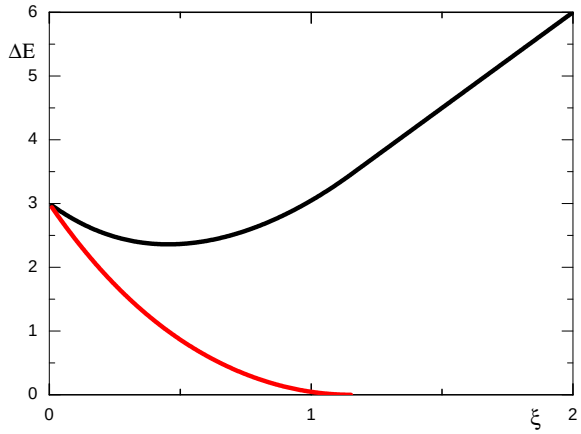

Figure 12: Changes of the energy barrier as a function of ξ with MA and $\sigma = 3$.

$t/2t_s(\sigma = 5)$	LA	TA	MA
WC	355.83	1.48	20.29
SC	1.04×10^6	11.57	505.99

Table I: Reduced switching times for the WC and SC for the three anisotropy configurations. $\xi = 0.3$ for WC. $\xi = 1.5$ for LA-SC and MA-SC. $\xi = 2.5$ for TA-SC

Fig. 12 shows the energy barrier as a function of ξ. The energy barrier along the second step of the process disappears at the critical value $\xi = 2/\sqrt{3}$, where the dynamics of the system becomes a one-step process. As the DDI increases to higher values, the energy barrier increases, leading to a constant increase in the switching time for high ξ, as can be seen in Fig. 13, where the switching time for SC is much higher than that of WC.

By way of comparison we gather in Table I some results for the DDI-MD. From this table, for $\sigma = 5$, we

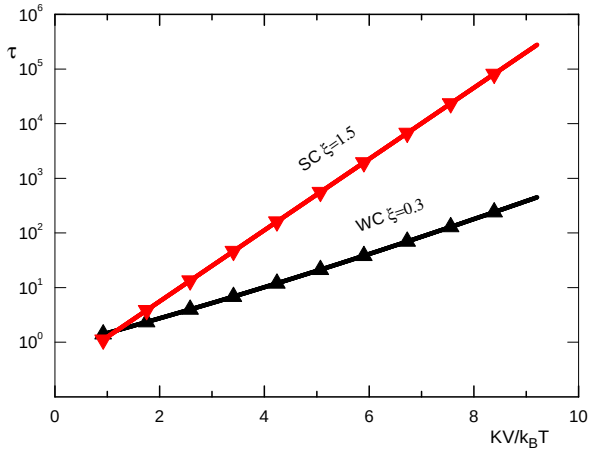

Figure 13: Reduced switching time τ of the DDI-MD with MA for weak and strong coupling regimes.

$t(\sigma = 8, \xi = 0.346)$	LA	TA	MA
	$3.42 \times 10^{-6} s$	$9.84 \times 10^{-10} s$	$7.07 \times 10^{-9} s$

Table II: Switching times for the atomic Cobalt dimer for each of the three anisotropy configurations.

see that for the three anisotropy configurations the switching time increases then decreases with the DDI coupling ξ. The fastest switching seems to occur for weak coupling and transverse anisotropy. This means that a magnetic dimer composed of two rather thin films should exhibit the fastest dynamics.

Table II shows the switching times for cobalt atoms in the three different anisotropies. The parameters used for the calculations are $\mu_a = 1.57 \times 10^{-23} Am^{-1} atom^{-1}$, $K_a = 2.53 \times 10^{-24} Jatom^{-1}$, $d = 2 \times 1.52 \times 10^{-10} m$ and $t_s = 1.76 \times 10^{-11} s$.

It is clearly seen that in this case TA leads to the shortest switching time. As such, in a chain of atoms a magnetic excitation should propagate faster if the anisotropy is normal to the chain axis.

V. DM COUPLED MAGNETIC DIMER

As discussed in section II A, DMI is also relevant in the present study and is investigated on the same footing as EI and DDI. Its effect is compared to that of the latter on the switching mechanisms of the MD. In order to investigate the effect of pure DMI, we consider the energy in Eq. (1) without the magnetic field and without the EI and DDI. In Ref.[17] it was shown that for a simple cubic lattice, on the $(1\,0\,0)$ surface the DMI vector D lies in the layer plane and thus induces perpendicular anisotropy. Accordingly, in Eq. (1) we drop the Zeeman energy, the EI and DDI contributions. We consider two situations where the DMI vector D lies in the MD plane and the anisotropy easy axes parallel or perpendicular to it.

A. D parallel to the anisotropy axes

After simplification, the reduced energy is a function of only the polar angles θ_1, θ_2 and is given by

$$\varepsilon(\theta_1, \theta_2) = -k\left(\cos^2\theta_1 + \cos^2\theta_2\right) + \delta \sin\theta_1 \sin\theta_2. \quad (55)$$

The anisotropy parameter $k = 0, 1$ is simply a switch introduced so as to be able to keep track of the anisotropy contribution in the subsequent results. Analysis of the stationary points yields

$$\begin{aligned} \varepsilon(0,0) = \varepsilon(\pi,\pi) &= \varepsilon(0,\pi) = \varepsilon(\pi,0) = -2k, \\ \varepsilon(\pm\frac{\pi}{2}, \pm\frac{\pi}{2}) &= \delta, \quad \varepsilon(\pm\frac{\pi}{2}, \mp\frac{\pi}{2}) = -\delta, \\ \varepsilon(\pm\frac{\pi}{2}, \mp \arcsin\left(\frac{\delta}{2k}\right)) &= -k\left[1 + \left(\frac{\delta}{2k}\right)^2\right]. \end{aligned}$$

From this analysis, we find that there is a critical value for the DMI which separates the weak and the strong coupling regimes. In our normalization with respect to the anisotropy energy [see Eq. (10)] this critical value is $\delta/k = 2$, see Fig. 15 (left).

1. *Weak coupling* $\delta/k < 2$

The minima are the FM and AFM states in the direction of anisotropy

$$(\theta_1, \theta_2) = (0,0), (\pi,\pi), (0,\pi), (\pi,0),$$

the maxima are at

$$(\theta_1, \theta_2) = \left(\pm\frac{\pi}{2}, \pm\frac{\pi}{2}\right),$$

and the saddle points are

$$\begin{aligned} \left(\theta_1^{(s)}, \theta_2^{(s)}\right) &= \left(\pm\frac{\pi}{2}, \mp\arcsin\left(\frac{\delta}{2k}\right)\right), \\ \left(\theta_1^{(s)}, \theta_2^{(s)}\right) &= \left(\mp\arcsin\left(\frac{\delta}{2k}\right), \pm\frac{\pi}{2}\right). \end{aligned}$$

The energy potential surface is shown in Fig. 14 (a). It can be seen that the net magnetic moment goes from, say the minimum $(0,0)$ to the minimum (π,π) through a two-step process that can proceed along two symmetrical paths. Each one of these goes through the first saddle point $\left(-\frac{\pi}{2}, \arcsin\left(\frac{d}{2k}\right)\right)$, passes into the local minimum $(\pi, 0)$ and crosses the saddle point $\left(-\pi - \arcsin\left(\frac{\delta}{2k}\right), -\frac{\pi}{2}\right)$.

The switching rates corresponding to these two steps have the expression

$$\Gamma^{(i)} = |\kappa_i| \sqrt{\frac{\sigma}{2\pi}} e^{-\frac{\sigma}{4}\left(4-\delta^2\right)}, \quad i = 1, 2. \quad (56)$$

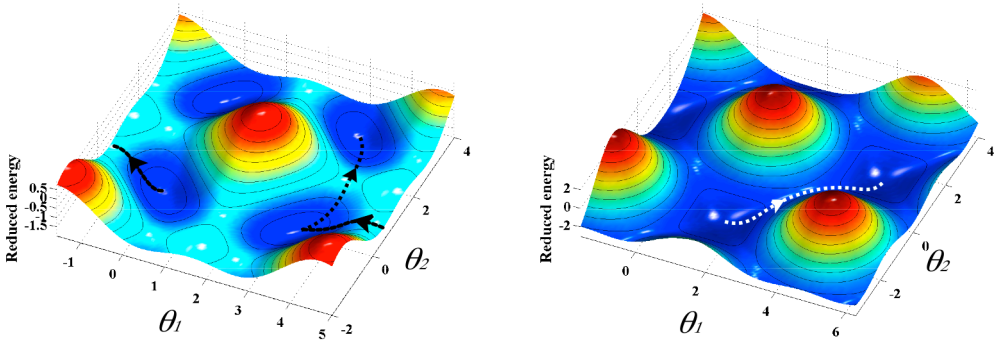

(a) Weak Coupling $\delta = 1$

(b) Strong Coupling $\delta = 3$

Figure 14: Energy potential surface of the different regimes for the DMI-MD with LA.

where the attempt frequencies κ_i are computed numerically. Upon counting the symmetry factors, we obtain the total switching rate

$$\Gamma_{\text{LAWC}}^{DMI} = 2|\kappa| \sqrt{\frac{\sigma}{2\pi}} e^{-\frac{\sigma}{4}(4-\delta^2)}. \tag{57}$$

2. *Strong Coupling*

In this regime, the DMI wins against the anisotropy field leading to a minimum with perpendicular magnetic moments, lying in the plane normal to the anisotropy axes since the DMI vector **D** is oriented along the latter. As such, the minima are

$$(\theta_1, \theta_2) = \left(\pm\frac{\pi}{2}, \mp\frac{\pi}{2}\right)$$

while the states

$$(\theta_1, \theta_2) = \left(\pm\frac{\pi}{2}, \pm\frac{\pi}{2}\right)$$

are maxima and the saddle points now are

$$(\theta_1, \theta_2) = (0,0), (\pi,\pi), (0,\pi)(\pi,0). \tag{58}$$

Hence, the system may escape from the state $\left(-\frac{\pi}{2}, \frac{\pi}{2}\right)$ into the state $\left(\frac{\pi}{2}, -\frac{\pi}{2}\right)$, thus reversing its resultant magnetic moment, along two different paths comprising the saddle points $(0,0)$ and (π,π). The switching rate of escape via one of these paths is given by

$$\Gamma_{\text{LASC}}^{DMI} = \alpha \left(\frac{2}{\pi}\right)^{3/2} \sqrt{\frac{\delta}{2\sigma}} \frac{\delta-2}{\delta+2} e^{-\sigma(\delta-2)}. \tag{59}$$

As is usually the case in the SC regime, the attempt frequency has been obtained analytically.

Fig. 14 shows the $3D$ energy potential surfaces for both WC and SC regimes. In Fig. 15 we plot the energy barrier (left) and the switching time (right) for the DMI-MD in the case of **D** parallel to the anisotropy axes. It is seen that the energy barriers for the two steps in the WC regime are equal and decrease quadratically with the DMI strength δ [see the argument of the exponential in Eq. (57)]. At the critical value of the DMI coupling, $\delta_c/k = 2$, the energy barrier vanishes and immediately after that it increases linearly with δ/k, as can be seen in Eq. (59).

Here again we see that the stronger is the coupling the slower is the MD switching. Note that in this regime, the saddle point corresponds to the state with the two magnetic moments along the easy axes and, more importantly, parallel to the DM vector **D**. To go through this saddle point the magnetic moments have to break free from the interaction and also to circumvent the anisotropy due to the DM interaction. This implies that the DMI leads to a longer switching time than the EI [see below]. Indeed, in the latter case switching is achieved against the (exchange) coupling while in the former it is achieved against the (DMI) coupling and the induced anisotropy.

VI. MOST EFFICIENT COUPLING IN A MAGNETIC DIMER

In this section we present a pairwise comparison of the different interactions with regard to their effect on the MD switching and on the corresponding switching time. On one hand, we have the short-range interactions EI and DMI, symmetric and antisymmetric, respectively. On the other hand, we have the long-range and antisymmetric interaction DDI. We first compare the EI with DDI and investigate the effects pertaining to the MD bond. Then, comes the comparison between the spins scalar-product and vector-product interactions, *i.e.* EI and DMI. Finally, we compare the DDI and DMI.

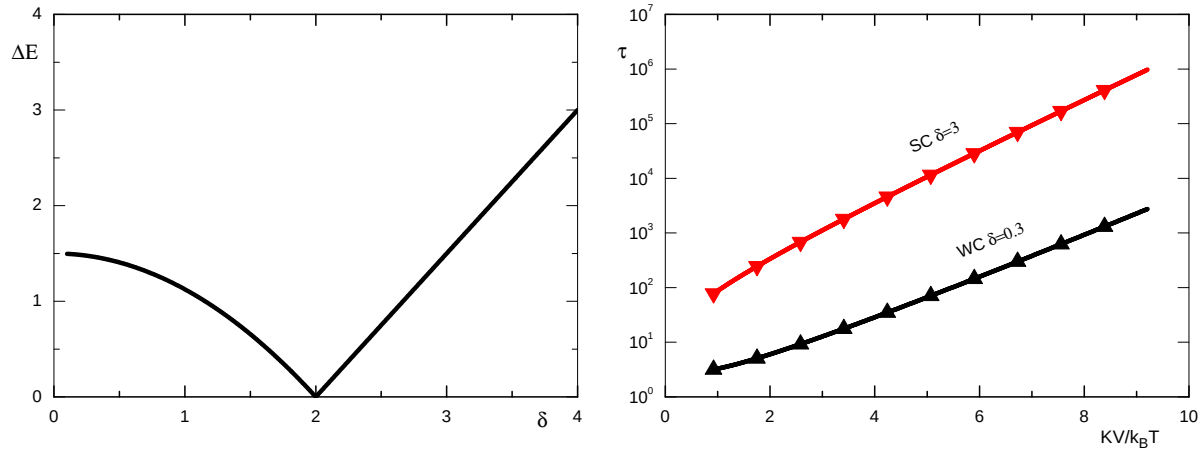

Figure 15: Energy Barrier (left) and reduced switching time (right) of the DMI magnetic dimer with LA for WC and SC.

A. EI versus DDI

For the EI-MD, when the exchange coupling exceeds the critical value the energy barrier [see Fig. 2 of Ref.[11]] becomes independent of the exchange coupling as soon as the saturated ferromagnetic state is reached. For the DDI-MD, the situation is fundamentally different because the energy barrier continues to increase as the DDI coupling increases, see *e.g.* Eq. (36) for the SC regime, where $\Delta\mathcal{E} = \sigma(1+\xi)$. This is due to the fact that the distance between the two magnetic moments, belonging to the layers or to the magnetic nanoparticles, plays a crucial role. Indeed, this distance cannot be smaller than a certain minimal value that corresponds to the thickness of the nonmagnetic spacer (in the case of two magnetic layers), or to the sum of radii of the two particles, or to the inter-atomic distance. Therefore, it is understood that the ξ axis must be cut off at a given value because the unlimited increase of ξ simply reflects the unphysical asymptotic limit $d \to 0$.

Let us now compare the switching times of the MD with LA when coupled via EI or DDI, in both the WC and SC regimes. The results are shown in Fig. 16 where the (reduced) switching time is plotted as a function of $\sigma = KV/k_{\mathrm{B}}T$. For these calculations, both the EI-MD and DDI-MD switch from the same initial state $(0,0)$ into the same final state (π,π).

As was discussed earlier, apart from the fact that the switching time obviously increases with σ (or with decreasing temperature) for both EI-MD and DDI-MD, we see that for both coupling regimes there is a critical value σ_c at which the switching times corresponding to EI and DDI intersect each other. Indeed, the DDI is always faster than the EI for low values of σ (below σ_c) and the situation reverses for values of σ higher than σ_c. The EI energy barrier is constant while that of DDI continues to grow. So, below σ_c the prefactor of the switching time prevails and the DDI is more favorable for a fast switching. However, as σ_c is exceeded, the energy barrier prevails over the prefactor and thereby the ever growing DDI energy barrier leads to a slower switching than via EI. The expression of σ_c is obtained in terms of the ratio of the switching rates in Eqs. (16) and (36), which is of the form $\mathrm{Prefactor}/e^{\sigma\xi}$ with

$$\mathrm{Prefactor} = \frac{\kappa}{\sqrt{2}}\sqrt{\frac{j\,(j-1)\,(\xi+2)}{\xi\,(3\xi-2)}}\,\frac{3\xi+2}{j+1}$$

where

$$\kappa \;=\; 1-\frac{\xi}{2}-\sqrt{\left(\frac{3}{2}\xi+1\right)^2+\frac{2}{\alpha^2}\xi\,(12+\xi)}.$$

More precisely, we have

$$\sigma_c\,(j,\xi,\alpha) \;=\; \frac{1}{\xi+1}\ln\left(\mathrm{Prefactor}\right).$$

The critical value σ_c is a decreasing function of the ratio ξ/j, which is simply due to the fact that the stronger the DDI the smaller is σ_c at which the energy barrier prevails over the prefactor of the switching time.

In conclusion, at low temperature, the EI-MD switches faster than DDI-MD.

B. EI versus DMI

Fig. 17 shows a comparison between the reduced switching times of the EI-MD and the DMI-MD in the weak coupling regime.

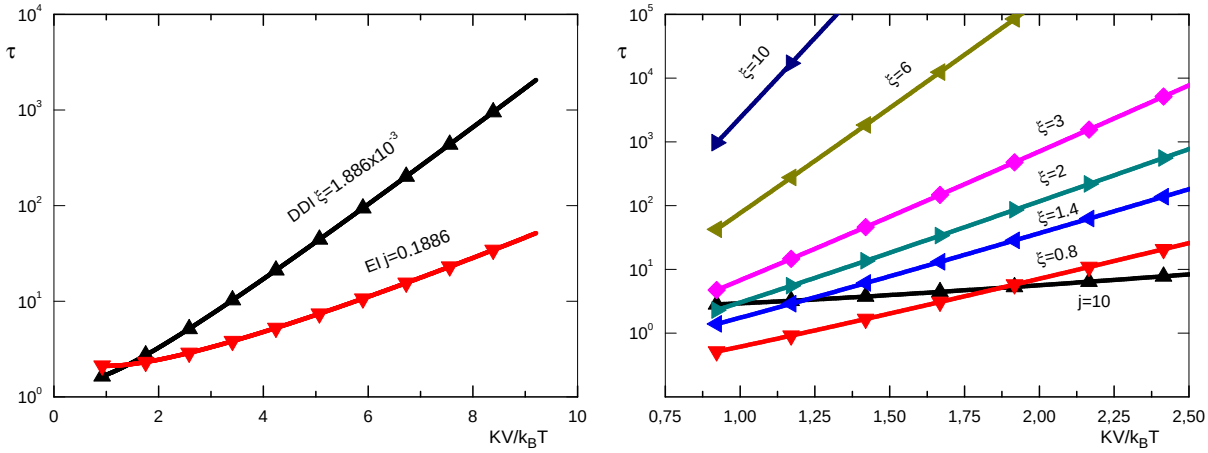

Figure 16: Reduced switching time, τ, versus $\sigma = KV/k_BT$ for the EI- and DDI-MD, in the absence of the magnetic field, for weak-coupling regime (left) and strong-coupling regime (right).

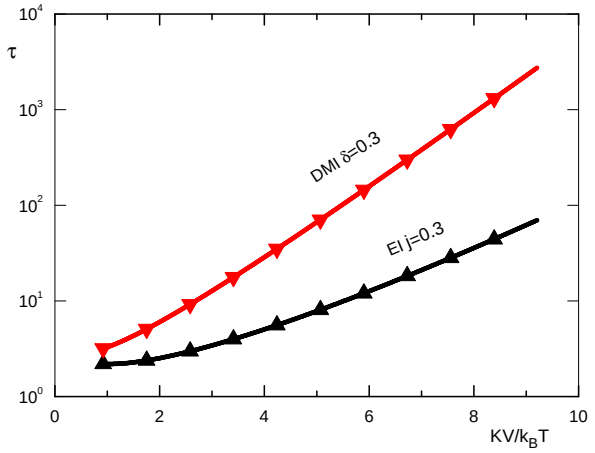

Figure 17: Reduced switching time, τ, versus $\sigma = KV/k_BT$ for the EI and DMI-MD, in the absence of the magnetic field, for weak-coupling regime.

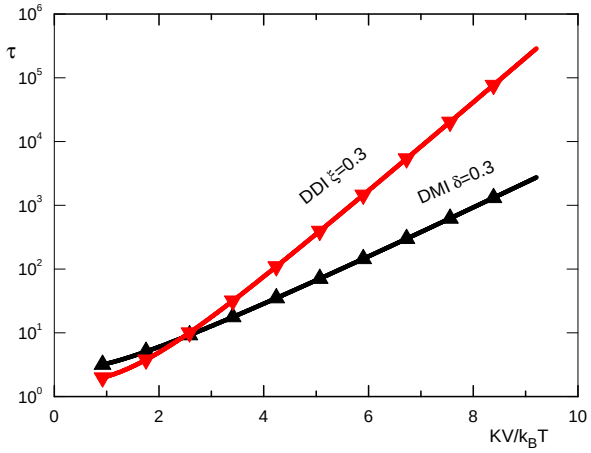

Figure 18: Reduced switching time, τ, versus $\sigma = KV/k_BT$ for the DDI-MD and DMI-MD, in the absence of the magnetic field, for weak-coupling regime.

The initial and final states are identical for both interactions and are given by $(\theta_1, \theta_2) = (\pi, \pi)$ (initial state), $(\theta_1, \theta_2) = (0, 0)$ (final state).

Unlike the previous cases (Fig. 16) there is no intersection of the two curves at finite values of σ in a range where our approach is applicable, *i.e.* where the second-order expansion of the energy is applicable.

From these results we see that the EI-MD has a shorter switching time than the DMI-MD. Indeed, in the weak coupling regime, for the dimer to switch one of its magnetic moments has to cross a saddle point into an intermediate state. In so doing, it has to circumvent the energy barrier associated with its coupling to the second moment. In the case of the DM coupling, in addition to the breaking free from the coupling there is a constraint related with the orientation imposed by the DM vector D, *i.e.* the inherent anisotropy.

C. DDI versus DMI

In Fig. 18, we compare the reduced switching times of the DDI-MD and the DMI-MD in the weak coupling regime. Two different curves for each interaction are presented.

The initial and final state are identical for both interactions and are given by $(\theta_1, \theta_2) = (\pi, \pi)$ (initial state), $(\theta_1, \theta_2) = (0, 0)$ (final state).

We first see that there exists a σ_c and that DDI leads to a faster switching than the DMI for $\sigma < \sigma_c$.

Switching in both cases is performed against the spin coupling and the anisotropy. However, the latter

has a stronger effect in the case of the DMI dimer.

VII. CONCLUSION

We have considered a magnetic dimer as a model system of two magnetic moments, atomic or macroscopic, coupled by either exchange, dipole-dipole, or Dzyalozhinski-Moriya interaction. This is a quite general system since the two magnetic moments may be those of two thin layers coupled by an effective interaction through a non magnetic spacer, two magnetic nanoparticles in a hosting matrix or on a substrate, or still two atomic magnetic moments. We have identified various coupling regimes and investigated the switching mechanisms of the system in each regime and in different anisotropy configurations. In each situation, we have computed the energy barrier and, for the high-to-intermediate damping, we used Langer's approach to compute the switching rate and, in some cases, provided the corresponding analytical expressions.

We have investigated how the energy barriers are affected by the coupling. For instance, for the dipole-dipole interaction we find that the energy barrier may either increase or decrease with the coupling depending on the coupling regime. In the weak-coupling regime, we find that the switching rate, as a function of temperature, does not follow the simple Arrhenius law because the prefactor dominates over the exponential. Furthermore, transverse anisotropy or equivalently, rather thin magnetic films, seem to exhibit the fastest switching process, as compared with the longitudinal or mixed anisotropy.

We then compared the three interactions with regard to their efficiency in switching the magnetic dimer. Comparing exchange and DDI led to the conclusion that below some critical temperature the exchange-coupled MD switches faster than the dipolar-coupled MD. Next, comparing the isotropic and anisotropic exchange and Dzyaloshinskii-Moriya interactions we have seen that in the latter case the inherent anisotropy makes the switching longer. Altogether, we have

$$\tau_{\rm EI} < \tau_{\rm DMI} < \tau_{\rm DDI}$$

which is compatible with the fact that the corresponding couplings are ordered in the following way

$$\lambda_{\rm EI} > \lambda_{\rm DMI} > \lambda_{\rm DDI}$$

and that $\tau \sim 1/\lambda$.

In a pure material, *i.e.* without too many impurities, it turns out that the fastest recovering of the magnetic state and thereby that of the system magnetization occurs via the exchange coupling. In this work, we provide details of how this switching occurs.

We have already started a few experiments for investigating the dynamics of coupled thin films grown by our collaborators. We intend to perform various measurements of FMR with varying field and frequency using a network analyzer. In addition, the slow dynamics of the dimer may be probed by measuring the isothermal and thermoremanent magnetization by a commercial SQUID in a wide range of temperature.

For a closer comparison with experiments we need to consider more general situations with arbitrary directions of the two anisotropy axes in an oblique magnetic field. Such calculations will be performed numerically in a subsequent work.

Appendix A: Details for WC of DDI-MD with MA

The stationary states are given by

$$\begin{aligned}\theta_1, \theta_2 &= \frac{\pm_a \arccos x_+ \pm_b \arccos x_-}{2} \\ \theta_1, \theta_2 &= \pm_c \pi + \frac{\pm_d \arccos x_+ \pm_e \arccos x_-}{2} \end{aligned} \quad \text{(A1)}$$

where

$$\begin{aligned} x_+^+ &= \pm 1, \quad x_-^+ = \pm 1, \\ x_+^- &= \pm\sqrt{\frac{36\xi^2+9\xi^4}{36\xi^2+16}}, x_-^- = \pm\sqrt{\frac{9\xi^4+4\xi^2}{16+4\xi^2}}. \end{aligned}$$

and the subindex $a...e$ indicates independence between different $\pm, \mp$ signs.

In the weak coupling, the minima of the MD are located at

$$\begin{aligned}\theta_1 &= \pm\frac{\arccos x_+^- - \arccos x_-^-}{2}, \\ \theta_2 &= \pm\frac{\arccos x_+^- + \arccos x_-^-}{2}\end{aligned}$$

and

$$\begin{aligned}\theta_1 &= \mp\pi \mp \frac{\arccos x_+^- - \arccos x_-^-}{2}, \\ \theta_2 &= \pm\pi \mp \frac{\arccos x_+^- + \arccos x_-^-}{2}\end{aligned}$$

where the sign of $x_\pm^-$ is taken as positive. The maxima are at

$$\begin{aligned}\theta_1 &= \pm\frac{\arccos x_+^- - \arccos x_-^-}{2}, \\ \theta_2 &= \pm\frac{\arccos x_+^- + \arccos x_-^-}{2}\end{aligned}$$

and

$$\begin{aligned}\theta_1 &= \pm\pi \mp \frac{\arccos x_+^- + \arccos x_-^-}{2}, \\ \theta_2 &= \pm\pi \mp \frac{\arccos x_+^- - \arccos x_-^-}{2}\end{aligned}$$

where the sign of $x_{\pm}^{-}$ is taken as negative. Hence, the saddle point are at

$$\begin{aligned}(\theta_1,\theta_2) &= (0,\pm\pi),(\pm\pi,0),(\pm\pi,\pm\pi),\\ &\quad (\pm\pi,\mp\pi),\left(\pm\frac{\pi}{2},\pm\frac{\pi}{2}\right),\left(\pm\frac{\pi}{2},\mp\frac{\pi}{2}\right).\end{aligned}$$

The switching rates for the first and second step in the WC regime read

$$\begin{aligned}\Gamma^{(1)}_{\mathrm{MAWC}} &= \frac{|\kappa|}{2\pi}\sqrt{\frac{W_+^1W_-^1}{(\xi+2r)\,|\xi-2r|\,(1+\xi+r)}}\sqrt{\frac{V_+^1V_-^1}{(1+\xi-r)}}e^{\sigma+\sigma\xi+\varepsilon_m^1(0)},\\ \Gamma^{(2)}_{\mathrm{MAWC}} &= \frac{|\kappa|}{4\pi}\sqrt{\frac{W_+^2W_-^2}{(2\xi+r_p)\,(1+2\xi+r)}}\sqrt{\frac{V_+^2V_-^2}{|2\xi-r_p|\,(1+2\xi-r_p)}}e^{\sigma+2\sigma\xi+\varepsilon_m^2(0)},\end{aligned}\tag{A2}$$

where

$$\varepsilon_m^j(0)=-\sigma\left(1+\left(C_{p1}^j\right)^2-\left(C_{p2}^j\right)^2\right)-\sigma\xi\left(2C_{p1}^jC_{p2}^j+Q_p^j\right),$$

$$V_\pm^j=N_V^j\pm\frac{1}{2}R_P^j,\quad W_\pm^j=N_t^j\pm R_t^j,$$

$$N_t^j=\left[\left(C_{p1}^j\right)^2-\left(C_{p2}^j\right)^2\right]+\xi C_{p1}^jC_{p2}^j+\frac{\xi}{2}Q_p^j,\quad N_V^j=-\frac{1}{2}\left(1-\left(C_{p2}^j\right)^2\right)-\frac{\xi}{2}Q_p^j,$$

$$\begin{aligned}R_t^j &= \sqrt{\left(1-\left(C_{p1}^j\right)^2-\left(C_{p2}^j\right)^2\right)^2+\frac{\xi^2}{4}\left(C_{p1}^jC_{p2}^j+2Q_p^j\right)^2},\\ R_P^j &= \sqrt{\left(1-\left(C_{p2}^j\right)^2\right)^2+\xi^2\left(Q_p^j\right)^2},\quad Q_p^j\equiv\sqrt{\left(1-\left(C_{p1}^j\right)^2\right)\left(1-\left(C_{p2}^j\right)^2\right)},\end{aligned}$$

with

$$\begin{aligned}r &= \sqrt{\xi^2+1},\quad r_p=\sqrt{\xi^2+4},\\ C_{pi}^j &\equiv \cos\theta_i^j.\end{aligned}$$

$i=1,2$ refers to the i^{th} layer and $j=1,2$ refers to the j^{th} minimum.

[1] E. F. Kneller and R. H. Hawig, IEEE Trans. Magn. **27**, 3588 (1991).
[2] R. H. Victora, X. Shen, IEEE Trans. Magn. **41**, 537 (2005).
[3] D. Suess, T. Schrefl, R. Dittrich, M. Kirschner, F. Dorfbauer, G. Hrkac, J. Fidler, J. Magn. Magn. Mater. **290**, 551 (2005).
[4] J. F. Cochran, J. Rudd, W. B. Muir, B. Heinrich, and Z. Celinski, Phys. Rev. B **42**, 508 (1990).
[5] M. Grimsditch, S. Kumar, and E. E. Fullerton, Phys. Rev. B **54**, 3385 (1996).
[6] R. Zivieri, L. Giovannini, and F. Nizzoli, Phys. Rev. B **62**, 14950 (2000).
[7] H. N. Bertram and J. C. Mallinson, J. Appl. Phys. **40**, 1301 (1969).
[8] H. N. Bertram and J. C. Mallinson, J. Appl. Phys. **41**, 1102 (1970).
[9] A. Lyberatos and R.W. Chantrell, J. Appl. Phys. **73**, 6501 (1993); D. Cimpoesu, A. Stancu, I. Klik, C.-R. Chang, and L. Spinu, J. Appl. Phys. **109**, 07D339 (2011).
[10] D. Rodé, H. N. Bertram and D. R. Fredkin, IEEE Trans. Magn. **MAG-23**, 2224 (1987).
[11] H. Kachkachi, Eur. Phys. Lett. **62**, 650 (2003); *ibid*, J. Mol. Liquids **114**, 113 (2004).
[12] J.S. Langer, Phys. Rev. Lett. **21**, 973 (1968); *ibid*, Ann. Phys. (N.Y.) **54**, 258 (1969).

[13] S. Titov, H. Kachkachi, Yu. Kalmykov, W.T. Coffey, Phys. Rev. B **72**, 134425 (2005).
[14] I. Solomon, Phys. Rev. **99**, 559 (1955).
[15] I. Dzyaloshinsky, J. Phys. Chem. Solids **4**, 241 (1958).
[16] T. Moriya, Phys. Rev. Lett. **4**, 228 (1960); *ibid*, Phys. Rev. **120**, 91 (1960).
[17] A. Crépieux and C. Lacroix, J. Magn. Magn. Mater. **182**, 341 (1998).
[18] K. Xia, W. Zhang, M. Lu, and H. Zhai, Phys. Rev. B **55**, 12561 (1997).
[19] H.-B. Braun, J. Appl. Phys. **76**, 6310 (1994).
[20] D. A. Garanin, E. Kennedy, D. S. F. Crothers, and W. T. Coffey, Phys. Rev. E **60**, 6499 (1999).
[21] W.T. Coffey, D.A. Garanin, and D.J. McCarthy, Adv. Chem. Phys. **117**, 483 (2001).
[22] H. Kachkachi, J. Mol. Liquids **114**, 113 (2004).
[23] See Ref.[12] for a rigorous derivation
[24] Indeed, if the saddle point is to describe the nucleating fluctuation, there must be exactly one direction of motion away from the saddle point in which the solution of the equations of motion of the modes ψ_n is unstable[12].
[25] We thank Yu. Kalmykov for having reminded us to mention this issue. We also thank D. Garanin and O. Chubykalo-Fesenko for a discussion of related issues.